

AD-A057 236

Final

USADACS Technical Library



5 0712 01010454 4

AD

TECHNICAL REPORT ARCSL-TR-78038

INVESTIGATION INTO THE EFFECTS OF WEAPON SETBACK  
ON VARIOUS MATERIALS AND GEOMETRIES

TECHNICAL  
LIBRARY

by

Richard S. Simak

Munitions Division

July 1978

19970925 121

DTIC QUALITY INSPECTED 5



US ARMY ARMAMENT RESEARCH AND DEVELOPMENT COMMAND  
Chemical Systems Laboratory  
Aberdeen Proving Ground, Maryland 21010

Approved for public release, distribution unlimited.

Disclaimer

The findings in this report are not to be construed as an official Department of the Army position unless so designated by other authorized documents.

Disposition

Destroy this report when it is no longer needed. Do not return it to the originator.

**UNCLASSIFIED**

SECURITY CLASSIFICATION OF THIS PAGE (When Data Entered)

REPORT DOCUMENTATION PAGE		READ INSTRUCTIONS BEFORE COMPLETING FORM																
1. REPORT NUMBER ARCSL-TR-78038	2. GOVT ACCESSION NO.	3. RECIPIENT'S CATALOG NUMBER																
4. TITLE (and Subtitle) INVESTIGATION INTO THE EFFECTS OF WEAPON SETBACK ON VARIOUS MATERIALS AND GEOMETRIES		5. TYPE OF REPORT & PERIOD COVERED Technical Report March 1977-January 1978																
		6. PERFORMING ORG. REPORT NUMBER																
7. AUTHOR(s) Richard S. Simak		8. CONTRACT OR GRANT NUMBER(s)																
9. PERFORMING ORGANIZATION NAME AND ADDRESS Commander/Director, Chemical Systems Laboratory Attn: DRDAR-CLN-D Aberdeen Proving Ground, MD 21010		10. PROGRAM ELEMENT, PROJECT, TASK AREA & WORK UNIT NUMBERS Task 1T161101A91A/7HA91X47																
11. CONTROLLING OFFICE NAME AND ADDRESS Commander/Director, Chemical Systems Laboratory Attn: DRDAR-CLJ-R Aberdeen Proving Ground, MD 21010		12. REPORT DATE July 1978																
		13. NUMBER OF PAGES 38																
14. MONITORING AGENCY NAME & ADDRESS (if different from Controlling Office)		15. SECURITY CLASS. (of this report)  UNCLASSIFIED																
		15a. DECLASSIFICATION/DOWNGRADING SCHEDULE NA																
16. DISTRIBUTION STATEMENT (of this Report)  Approved for public release; distribution unlimited.																		
17. DISTRIBUTION STATEMENT (of the abstract entered in Block 20, if different from Report)																		
18. SUPPLEMENTARY NOTES																		
19. KEY WORDS (Continue on reverse side if necessary and identify by block number)																		
<table border="0"> <tr> <td>(U) Setback force</td> <td>Setback mathematics</td> <td>Stress duration</td> <td>Static testing</td> </tr> <tr> <td>Structural integrity</td> <td>Literature model</td> <td>Stress-strain relation</td> <td>Aluminum 24-ST</td> </tr> <tr> <td>Launch environment</td> <td>Predicted performance</td> <td>Critical velocity</td> <td>Motion equation</td> </tr> <tr> <td>Flight testing</td> <td>Mathematical model</td> <td>Ferrous alloys</td> <td>Viscous parameter</td> </tr> </table> <p align="center">(Continued on reverse side)</p>			(U) Setback force	Setback mathematics	Stress duration	Static testing	Structural integrity	Literature model	Stress-strain relation	Aluminum 24-ST	Launch environment	Predicted performance	Critical velocity	Motion equation	Flight testing	Mathematical model	Ferrous alloys	Viscous parameter
(U) Setback force	Setback mathematics	Stress duration	Static testing															
Structural integrity	Literature model	Stress-strain relation	Aluminum 24-ST															
Launch environment	Predicted performance	Critical velocity	Motion equation															
Flight testing	Mathematical model	Ferrous alloys	Viscous parameter															
20. ABSTRACT (Continue on reverse side if necessary and identify by block number)																		
<p>(U) The objective of this task was to develop a method for estimating the mechanical behavior of various materials when subjected to weapon (e.g., howitzer) setback forces. A mathematical model was developed for predicting the dynamic mechanical behavior of the materials, from which predictions concerning certain material-geometry combinations were made. Tests were carried out with aluminum and steel specimens and the resultant data compared with results</p> <p align="center">(Continued on reverse side)</p>																		

## 19. KEY WORDS (Contd)

Dynamic testing  
Lightweight alloys  
High-energy forming  
High-explosive forming  
Low-explosive forming  
Exploding-wire forming  
Magnetic-pulse forming  
Mechanical-pneumatic forming  
Air-activated-ram forming  
Strain hardening  
Dynamic mechanics

Plastic deformation  
High-velocity stress  
Strength factors  
Impact loading  
Displacement mechanisms  
Grain distortion  
Slip  
Twinning  
Metal flow  
Dislocation dipoles  
Geometric influence

## 20. ABSTRACT (Contd)

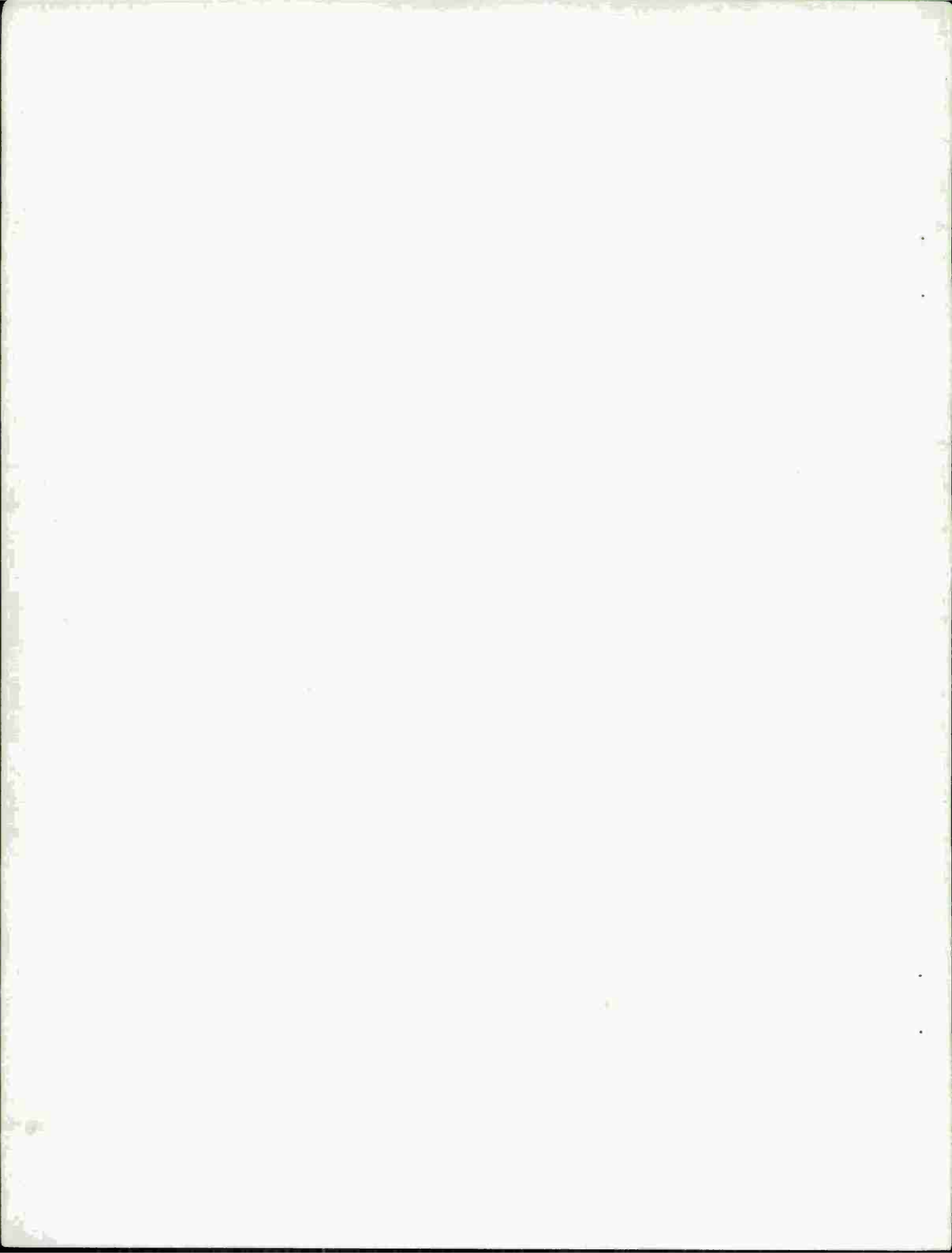
predicted by the mathematical model. The mathematical model selected was a viscoelastic model involving viscous, elastic, and in one instance, plastic parameters. This model accurately predicted the measured values in five material-geometry combinations actually tested. The methodology described in this report can be used to predict accurately the structural integrity of munition components when exposed to weapon setback environments.

## PREFACE

The literature search and experimental work described in this report were authorized under project/task 1T161101A91A/7HA91X47, an in-house independent research task, Investigation into the Effects of Weapon Setback on Various Materials and Geometries. This work was carried out from March 1977 to January 1978. Data are recorded in Notebook 9612.

The use of trade names in this report does not constitute an official endorsement or approval of the use of such commercial hardware or software. This report may not be used for purposes of advertisement.

Reproduction of this document in whole or in part is prohibited except with permission of the Commander/Director, Chemical Systems Laboratory, Attn: DRDAR-CLJ-R, Aberdeen Proving Ground, Maryland 21010; however, DDC and the National Technical Information Service are permitted to reproduce the document for US Government purposes.



## CONTENTS

	<u>Page</u>
I. INTRODUCTION . . . . .	7
II. BACKGROUND . . . . .	7
III. MODELING EFFECT . . . . .	9
IV. EXPERIMENTAL METHODS . . . . .	10
V. RESULTS . . . . .	13
VI. DISCUSSION OF RESULTS . . . . .	15
VII. CONCLUSIONS . . . . .	17
LITERATURE CITED . . . . .	19
GLOSSARY . . . . .	21
APPENDIXES	
A. Solution of the Dynamic Equation for the Elastic-Viscoelastic Model when Excited by a Half-Cycle Sine Pulse . . . . .	23
B. Propagation of Stress Wave in a Flat Plate . . . . .	27
C. Calculation of the AISI 1018 Low-Carbon Steel Circular Flat Plate . . . . .	31
D. The Response Characteristics of the Half-Cycle Sine Pulse . . . . .	35
DISTRIBUTION LIST . . . . .	37

## LIST OF FIGURES

### Figure

1 Mechanical Analog of Elastic-Viscoelastic Model . . . . .	9
2 Idealized True Stress-Strain Diagram . . . . .	10
3 Flat Plate Configuration . . . . .	11

LIST OF FIGURES (Contd)

<u>Figure</u>		<u>Page</u>
4	Solid Pin Configuration . . . . .	11
5	Calibration Chart for Shock Machine . . . . .	12
6	Statically Obtained True Stress-Strain Diagram . . . . .	14
7	Mechanical Analog for Elastic-Viscoelastic-Plastic Model . . . . .	16

LIST OF TABLES

<u>Table</u>		
1	Comparison Between Measured and Predicted Strengths . . . . .	13
2	Calculated Dynamic Material Constants . . . . .	15

# INVESTIGATION INTO THE EFFECTS OF WEAPON SETBACK ON VARIOUS MATERIALS AND GEOMETRIES

## I. INTRODUCTION.

The design of chemical munitions involves several factors and among them is the structural behavior of the components when subjected to various loads. In some cases the requirement is that the component withstand the maximum stress or weapon setback force while others require failure at minimum setbacks yet survive the logistical cycle. In either event, the structural integrity of the component must be evaluated as part of the development of an item.

At present, this evaluation involves the calculation of the component's structural integrity using statically obtained strength values, followed by bench testing, if possible, and the testing of munitions. The emphasis is on system testing which yields specific solutions for specific configurations, and if the configuration is changed the system must be retested. This method has resulted in increased project costs and, at times, in schedule slippages.

What is required is a reliable method for analyzing the effects of the launch environment on munition components. Therefore, an investigation was undertaken to develop such a method and, thereby, reduce the amount of munition flight testing and/or dynamic bench testing required with its associated costs.

This work was divided into two phases, the first of which was to develop a mathematical model which predicts the mechanical behavior of materials subjected to setback. This involved a literature search followed by a mathematical modeling effort. The second phase involved comparing the model prediction with experimental data which were generated as part of this effort.

## II. BACKGROUND.

Plastic deformation of solids was first considered in 1904 by Hopkinson who observed that iron and copper wires subjected to rapidly applied tensile stress could be stressed beyond the static elastic limit and breaking loads and still remain in the elastic range, providing that the duration of such stress was of the order of 0.001 second or less.<sup>1</sup> But it was not until 1941 when Von Karman and Taylor each independently established the theory of plastic strain propagation in metals that this phenomenon was seriously studied.<sup>2</sup> This theory assumes that stress is a unique function of strain and that this functional relationship can be obtained by solving the equation of motion for whatever case is under consideration. The original paper used the simple case of a slender rod subjected to longitudinal impact. Two important features of this theory are that the velocity of propagation is less than that of an elastic strain and that an upper or critical impact velocity exists above which the material fails.

Since the publication of this theory, a body of research data has grown; in general it can be placed into four categories:

(1) The determination of the dynamic properties of various materials. The materials tested have been mostly high-strength ferrous alloys<sup>3</sup> and lightweight alloys for use in the aerospace industry<sup>4</sup> with a small amount of data on annealed nonferrous alloys. In general, a material's strength increases when subjected to impact loads (relative to statically applied loads), but by varying relative amounts for various materials. For example, cold-rolled low-carbon steel has an ultimate strength of 87,750 psi under static conditions and 125,250 psi under dynamic conditions or a 43% increase while 24-ST aluminum has an ultimate strength of 65,150 psi under static conditions and 68,600 psi under dynamic conditions or only a 5% increase. It was also noted that the strain rate affects both the strength and ultimate elongation of a material.

(2) Various investigations into the behavior of materials subjected to impact loads. This work usually involves solving the equation of motion for a geometry of interest, having one or more "dynamic" parameters, usually viscous or flow parameters. This is followed by dynamic bench tests to determine the specific value of parameters for a specific material.

(3) High-energy-forming technology for manufacturing applications. This work is concentrated in two areas; the development of techniques for applying high-velocity stress waves and the development of process parameters. The techniques developed include both high- and low-explosive-forming, exploding-wire (capacitor rapidly discharging through a fine wire which vaporizes) forming, magnetic-pulse (quickly changing electromagnetic field) forming and mechanical-pneumatic (air-activated-ram) forming techniques.<sup>5</sup> The parametric process studies involved relating the depth of draw, material thickness, die diameter and standoff to the material's mechanical properties and the amount of forming energy involved.<sup>4</sup>

(4) Physical descriptions of the effect of impact loading of metals. The displacement mechanisms for metal subjected to impact loads are similar to that for statically applied loads, that is, grain distortion, slip\* and twinning.\*\* But in the case of impact loads, the deformation is greatest near the point of application and reduces with distance from that point.<sup>6</sup> There is also a time delay between the application of an impact load and the subsequent yielding. This phenomenon has been explained in part by the presence of foreign atoms in a metal lattice and grain boundaries, both of which constitute obstacles to the flow of metals.<sup>1</sup> Another obstacle to flow is strain hardening which is due to the buildup of dislocation dipoles† into a network which anchors dislocations.<sup>7</sup>

In summary: (1) The displacement mechanisms for metals subjected to impact loads are similar to those for statically applied loads, but with different distributions, (2) there exists a time delay between the application of impact loads and subsequent plastic yielding, (3) materials' strength increases when subjected to impact loads, but by varying relative amounts for various materials, and (4) previous investigations showed that flow or viscous parameters are important.

---

\* Slip is the displacement of one part of a crystal relative to another.

\*\* Twinning is the sliding of one plane of atoms over the adjacent plane.

† Dislocation dipole is the junction of one dislocation with another dislocation on an intersecting plane.

### III. MODELING EFFECT.

Based on the information obtained during the literature search a mathematical model has been developed to predict the time-dependent behavior of materials. This model assumes that materials behave in an elastic manner below the proportional limit (arbitrarily set at 2% elongation) and in a viscoelastic manner above the proportional limit. In addition, the viscoelastic element must have a time delay or, in this case, a viscous resistance feature which is known as a Voigt element. The mechanical analog of the model is given in figure 1, the equations for which are given to the right of the figure.

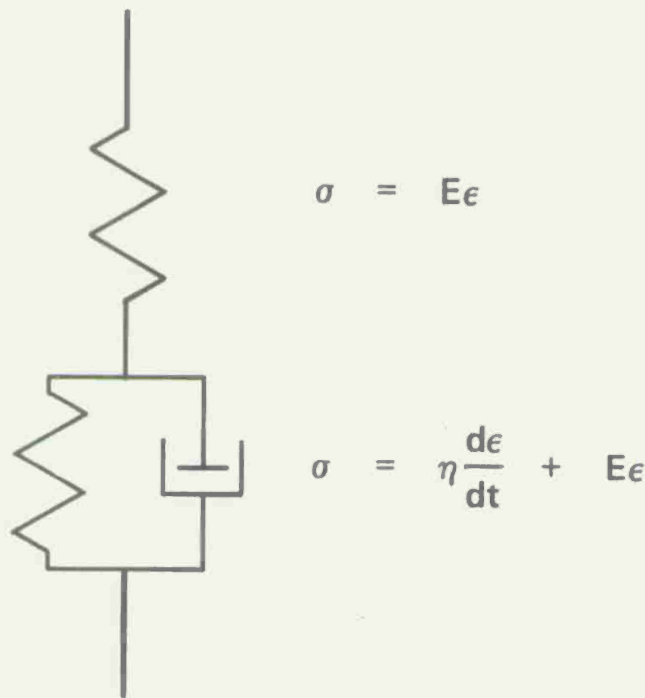


Figure 1. Mechanical Analog of Elastic-Viscoelastic Model

The response equation for this model is  $\sigma = (2E)\epsilon + \eta \frac{\partial \epsilon}{\partial t}$ \*. The time-dependent strain for this system is found by solving this equation for the model when excited by the forces due to the launch environments (which can be obtained from acceleration/pressure histories of the weapon system). Once the strain relationship is known, the other dynamic values can be determined. This involves taking the Laplace Transform of the dynamic equation, rearrangement and taking the inverse transform to find the time-dependent strain. The "dynamic modulus" is then the stress divided by the strain which is constantly changing with time.

\* See the glossary for definition of variables used here and in succeeding sections of this report.

The elastic and viscous constants of a material may be obtained from a statically obtained true stress-strain diagram by assuming that the material behaves elastically below the proportional limit and in a viscous manner above it. The graphical representation of this is shown in figure 2.

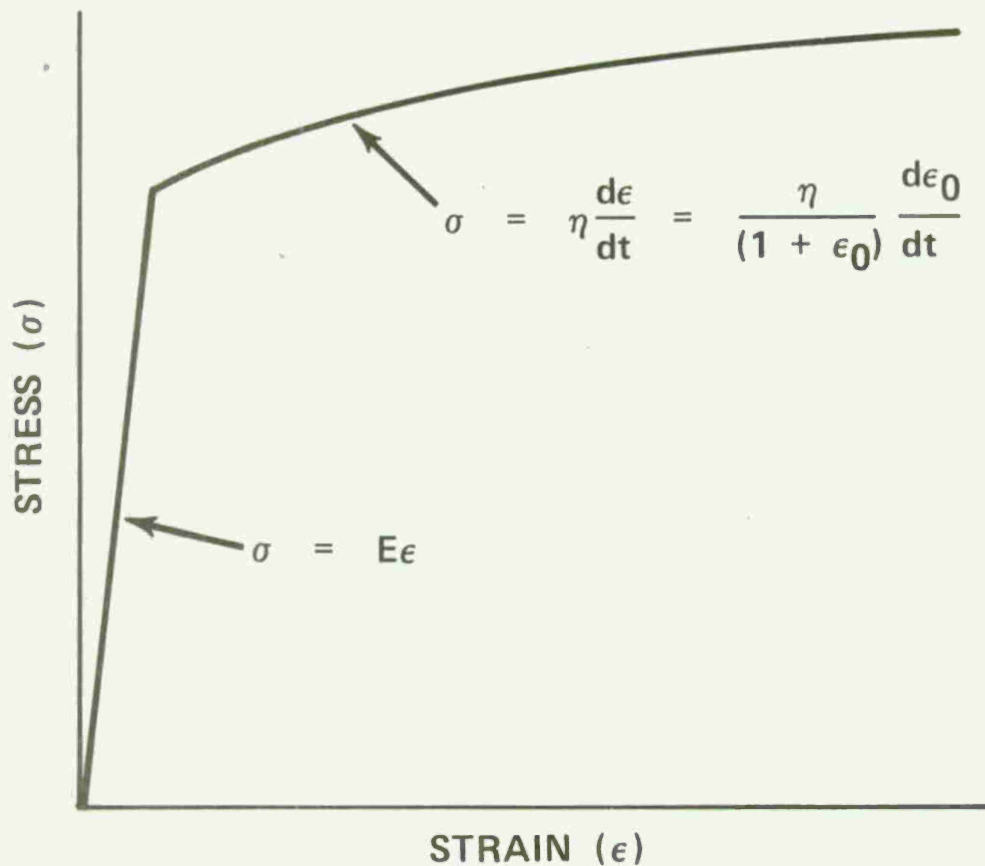


Figure 2. Idealized True Stress-Strain Diagram

#### IV. EXPERIMENTAL METHODS.

To compare the model predictions with experimental data a series of dynamic bench tests was performed involving two geometries (the thin flat plate as shown in figure 3 and the solid pin as shown in figure 4) and four materials (AISI 1018 and 1020 low carbon steel, type 316 austenitic stainless steel and 6061-T6 aluminum alloy). In addition, the stress-strain diagrams for all four materials were generated to provide elastic and viscous material constants.

The bench test machine used in this work was a Veripulse VP 400 Shock Machine which produces a controlled and reproducible acceleration at a constant pulse rate. The procedure for this testing involves securing a component holding fixture and weight to the bed of the shock machine and varying the bed drop height to achieve the proper acceleration while the neoprene compression pads control the pulse rate. The calibration chart for both pads is given in figure 5, and the estimated standard deviation for each pad is given in the results section of this

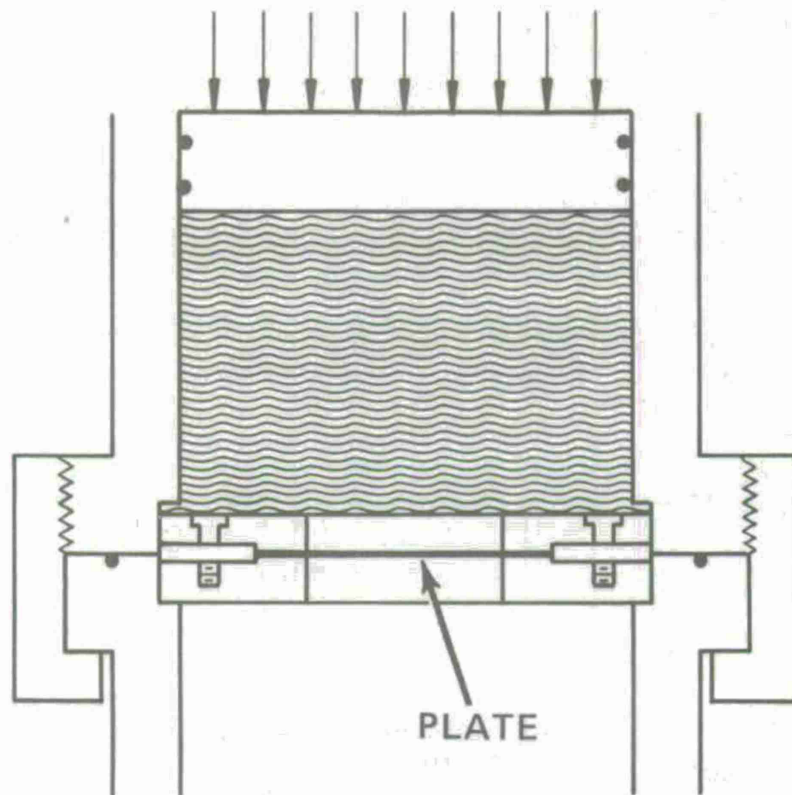


Figure 3. Flat Plate Configuration

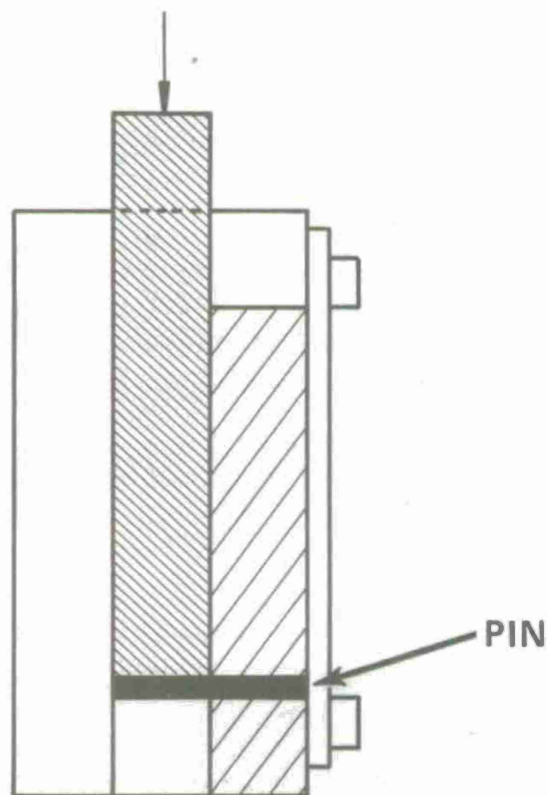


Figure 4. Solid Pin Configuration

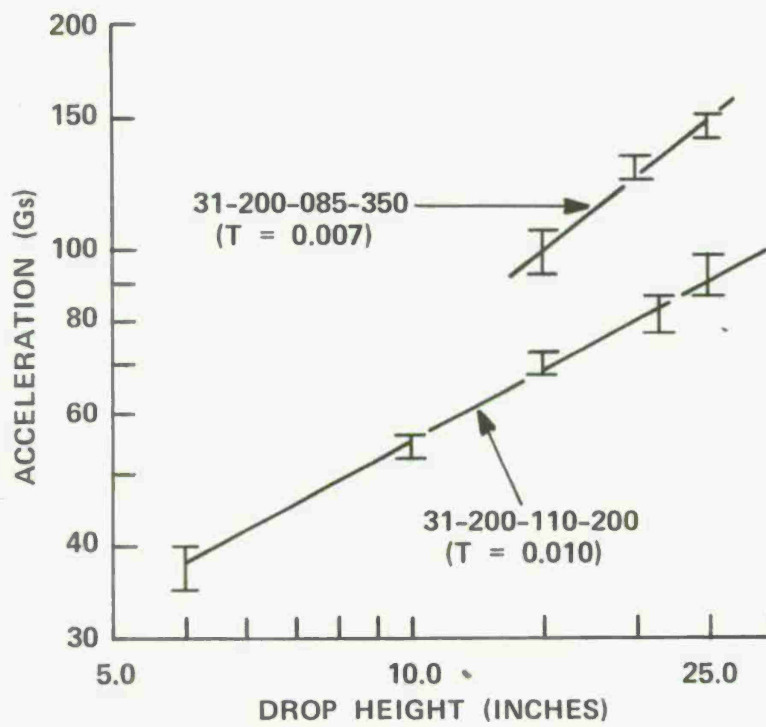


Figure 5. Calibration Chart for Shock Mixture

report. The acceleration history of this machine is a half sine wave pulse ( $a(t) = a_p \sin\left(\frac{\pi}{\tau}\right)t$ ). The "dynamic modulus" for the various materials can be estimated by solving the dynamic equation for the Elastic-Viscoelastic model when excited by the wave pulse, the solution of which is given in appendix A. Note that for loads of short duration, the modulus is dependent on the viscous constant rather than both material constants (elastic and viscous). The stress on a flat plate can then be found by solving the equation of motion for the flat plate given in appendix B. The stress on a solid pin can also be found by solving the equation of motion for that geometry, the solution of which is analogous to that for a flat plate, but with different boundary conditions ( $\alpha = \frac{\pi}{2\Lambda}$  and  $p = \frac{\pi c}{2\Lambda}$ ).

## V. RESULTS.

The results of the dynamic bench test effort are given in table 1. This work involved five material-geometry combinations and because of the go-no-go nature of the test setup only upper and lower strength values are reported. The Elastic-Viscoelastic-model predictions for all five combinations are also given in table 1. A sample calculation for 1018-flat plate combination is given in appendix C. For comparative purposes, strength predictions based on statically obtained material properties using standard formulas are included in table 1.

Table 1. Comparison Between Measured and Predicted Strengths

Material	Geometry	Bench-tested value	Model prediction	"Static prediction"
1018 Carbon steel	Flat plate (.0153 inch thick)	647-693 psi	697 psi	27 psi
1020 Carbon steel	Solid pin (.125 inch diameter)	1,048-1,082 lb	1,111 lb	388 lb
6061-T6 Aluminum	Flat plate (.025 inch thick)	508-555 psi	486 psi	59 psi
6061-T6 Aluminum	Solid pin (.1875 inch diameter)	1,048-1,119 lb	1,021 lb	714 lb
316 Austenitic steel	Solid pin (.1875 inch diameter)	2,484-2,552 lb	9,232 lb	1,898 lb

The statically obtained true stress-strain diagrams for all four materials are given in figure 6. From these diagrams the dynamic modulus ( $\sigma = \frac{\pi}{\tau} \eta$ ) and velocity of wave propagation  $\left[ c = \left( \frac{\phi_s}{\rho} \right)^{1/2} \right]$  were calculated and are given in table 2.

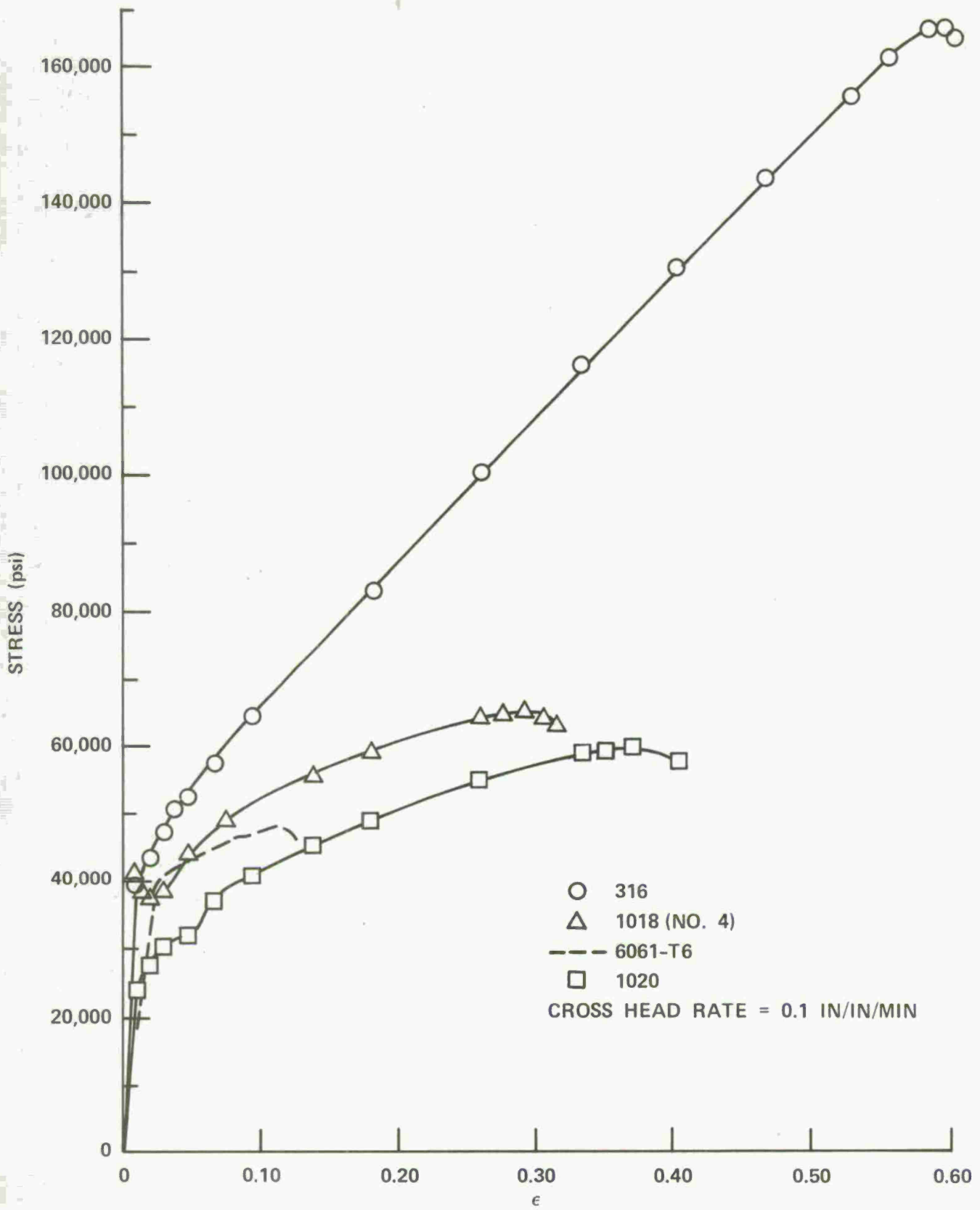


Figure 6. Statically Obtained True Stress-Strain Diagram

Table 2. Calculated Dynamic Material Constants

Material	Geometry	Dynamic modulus	Velocity of wave propagation
1018 Carbon steel	Flat plate	psi 4,358,000,000	ft 21,367
1020 Carbon steel	Solid pin	4,222,000,000	21,913
6061-T6 Aluminum	Flat plate	1,632,000,000	22,840
6061-T6 Aluminum	Solid pin	1,305,000,000	20,430
316 Austenitic steel	Solid pin	27,390,000,000	54,400

To estimate the precision of the Veripulse VP 400 Shock Machine, a series of instrumented tests was performed on both sets of neoprene compression pads. For pad 31-200-110-200, used in the 1020 steel and 6061-T6 aluminum solid pin tests, the standard deviation was 2.9 g acceleration or 49.0 lb load ( $F = ma = 16.9 \text{ lb} \times 2.9\text{g} = 49 \text{ lb}$ ). For pad 31-200-085-350, used in the flat plate and the 316 austenitic steel solid pin tests, the standard deviation was 4.6 g acceleration or 21.2 psi for the plates and 77.7 lb load for the pin.

## VI. DISCUSSION OF RESULTS.

For the low carbon steel the Elastic-Viscoelastic model predicted values slightly higher than the upper bench test value for both geometries tested (697 psi versus 693 psi for flat plate and 1,111 lb versus 1,082 lbs for the solid pin). For the 6061-T6 aluminum alloy the Elastic-Viscoelastic model predicted values slightly lower than the lower bench test value for both geometries tested (486 psi versus 508 psi for the flat plate and 1,021 lb versus 1,048 lb for the solid pin). In each case the difference between predicted and measured values are approximately the estimated standard deviation of the shock machine and consequently the differences may not be significant. In comparing the two methods of predicting strength values, it is seen that the predictions based on the Elastic-Viscoelastic model are far superior to those made using standard material strength values and formulas.

For the austenitic stainless steel type 316 the Elastic-Viscoelastic model predicted values considerably higher than the upper bench test value for the solid pin geometry (9,232 lb versus 2,522 lb). The most obvious explanation for this discrepancy is that the model as proposed does not adequately account for the behavior of 316 while it does so for low-carbon steel and the aluminum alloy.

In looking into the structure of the three metals some differences were found. Both the low-carbon steel and 6061-T6 aluminum alloy are basically pure metals doped with small percentages of other atoms to achieve certain desirable mechanical properties. Furthermore, both materials are subject to strain hardening.<sup>8</sup> Both the presence of impurities in the crystal lattice and the susceptibility to strain hardening tend to produce barriers to metal flow which can be modeled as a viscous drag element.

On the other hand, austenitic stainless steel type 316 is a mixture of iron (Fe), chromium (Cr) and nickel (Ni) where the Cr and Ni atoms substitute for Fe in the crystal lattice. Because of the high nickel content (10 to 14%) this steel does not appreciably strain-harden and is sometimes referred to as free spinning steel.<sup>9</sup> This relative lack of strain hardening has, in part, been explained by an "easy glide" mechanism where the density of dislocations rises linearly with plastic strain.<sup>7</sup> In fact, the presence of grain boundaries and impurities would be the only serious barrier to metal flow. Since the austenitic stainless steel does not follow the Elastic-Viscoelastic model previously stated, a new model for this material must be postulated. Based on the above discussion concerning 316, a three-element model shown in figure 7 is proposed. This model involves an elastic element to account for the behavior below the proportional limit followed by a Voigt element to account for grain boundary behavior followed by a friction element to account for the "easy glide" phenomenon. The equation of motion for this system is  $\sigma = (2E + \delta)\epsilon + \eta \frac{\partial \epsilon}{\partial t}$  whose equation is analogous to that for the Elastic-Viscoelastic model, i.e.,  $\phi = \frac{\pi}{\tau} \eta$ .

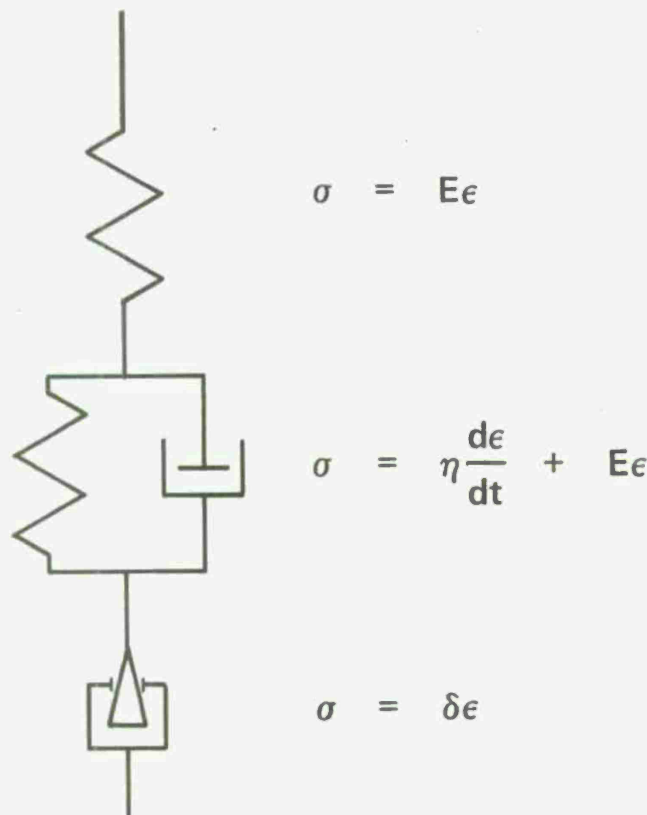
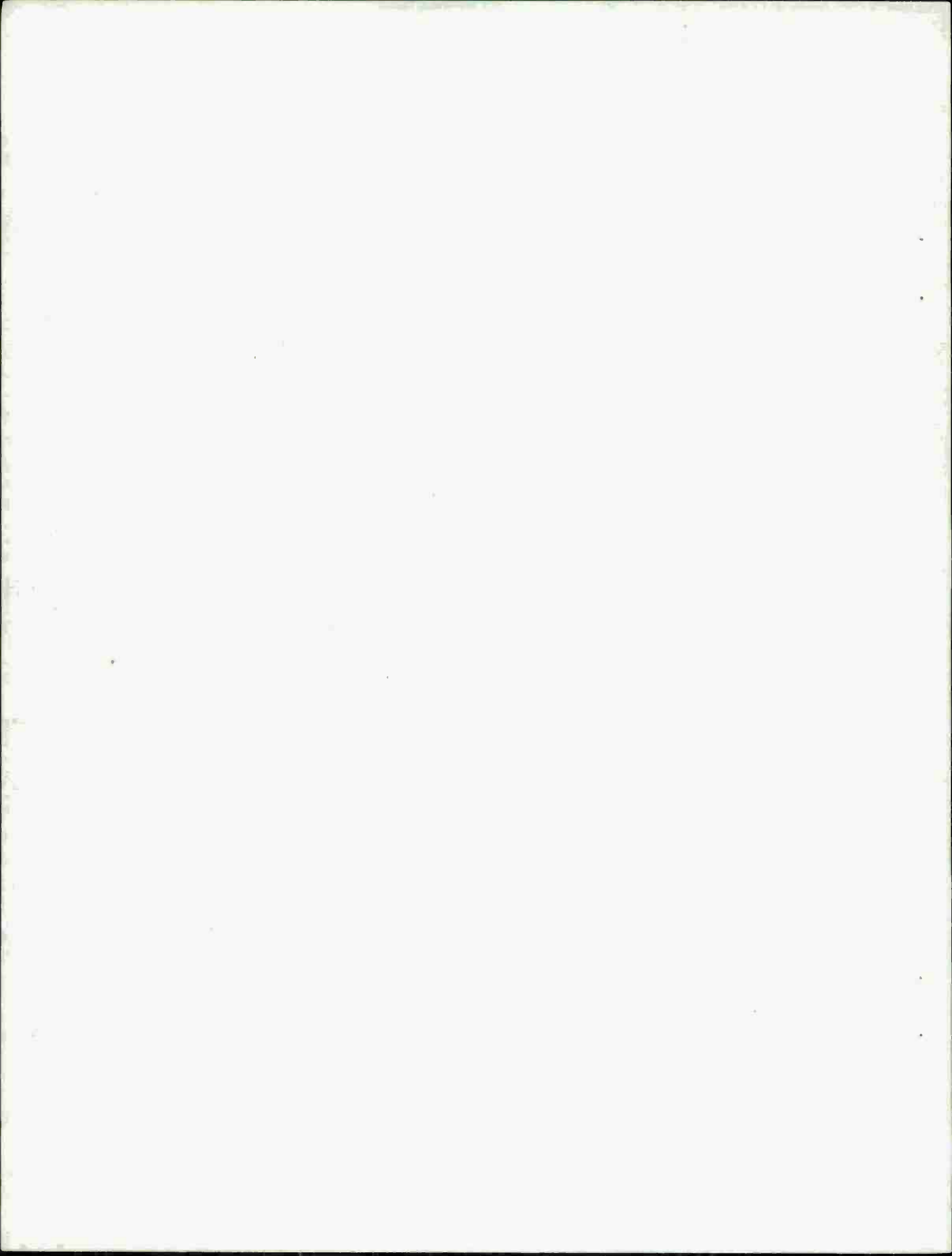


Figure 7. Mechanical Analog for Elastic-Viscoelastic-Plastic Model

In analyzing the true stress-strain diagram it is seen that 316 is elastic from 0 to .01 strain, viscoelastic from .01 to .039 and plastic from .039 to 59. For this case the viscous parameter  $\eta = \frac{50,400 - 39,500}{.0033} (1 + .039) = 3.4 \times 10^6$ ; likewise,  $\phi = 5.91 \times 10^8$  and  $c = 13,040$  ft/sec. Substituting this value of  $c$  into the equation of motion for the solid pin yields a predicted value of 2,861 lb. In comparing the three methods of predicting strength values it is seen that the prediction based on the three-element Elastic-Viscoelastic-Plastic model is superior to those made using both the standard formulas and two-element Elastic-Viscoelastic Model.

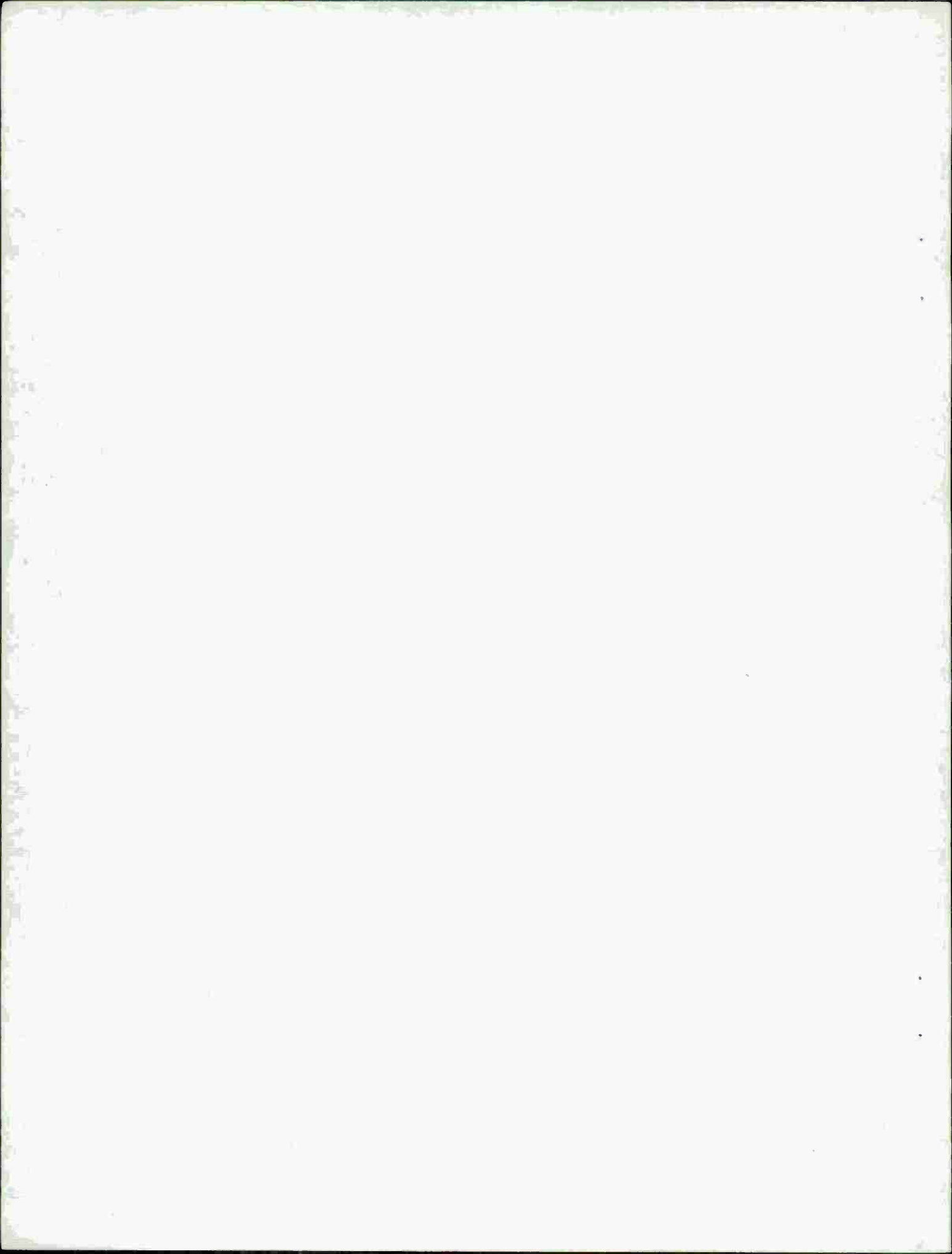
## VII. CONCLUSIONS.

The mechanical behavior of materials subjected to impact loads can be predicted by using relatively simple mechanical models to describe their behavior. The model parameters can be obtained from a true stress-strain diagram. In addition, the methodology used in the body of this report can be used to predict accurately the structural integrity of munition components.



## LITERATURE CITED

1. Clark, D. S. The Behavior of Metals Under Dynamic Loading. *Met. Prog.* 64(5), 67. (1953).
2. Von Karman, Theodore. OSRD No. 365, NDRC Rpt on The Propagation of Plastic Deformation in Solids. January 1942.
3. Clark, D. S., and Wood, D. S. The Tensile Impact Properties of Some Metals and Alloys. *ASM Trans. Q.* 42, 45-74 (1950).
4. Wood, W. W., *et al.* Final Report. Advanced Theoretical Formability, Manufacturing Technology. Contract No. AF33 (657) - 10823. USAF, Advanced Systems Manufacturing Technology Division. January 1965.
5. Bruno, E. J. ed. High-Velocity Forming of Metals. Society of Manufacturing Engineers, Dearborn, Michigan. 1968.
6. Rinehart, J. S. and Person, J. Behavior of Metals Under Impulsive Loads. Dover Publications, Inc. New York, New York. 1965.
7. McClintock, F. A. and Argan, A. S. Mechanical Behavior of Materials. Addison-Wesley Publishing Company, Reading, Massachusetts. 1966.
8. Guy, A. G. Introduction to Materials Science. McGraw-Hill Book Co., New York, New York. 1971.
9. Zapffe, C. A. Stainless Steel. American Society of Metals, Cleveland, Ohio. 1949.



## GLOSSARY

$\sigma$	stress
$\epsilon$	true strain = $\ln(1 + \epsilon_0)$
$\epsilon_0$	engineering strain
E	modulus of elasticity
$\eta$	viscous parameter
$\delta$	plastic modulus
$\rho$	density
A	shear area
I	moment of inertia
b	thickness
r	radius
$\nu$	Poisson's ratio
$\phi$	dynamic shear modulus = $\frac{\phi E}{2(1+\nu)}$
$\phi \epsilon$	dynamic tensile modulus
w	displacement
t	time
$\Lambda$	half wave length = $v_0 t$
$v_0$	impact velocity
$a_p$	peak acceleration
T	half sine wave period
F	force
M	moment

x	radial component of flat plate
y	circumferential component of flat plate
$c_0$	initial stress wave propagation velocity = $\left(\frac{\phi}{\rho}\right)^{1/2}$
$K_0$	radius of gyration = $\left(\frac{I}{A}\right)^{1/2}$
$\alpha$	wave number
P	pressure
p	angular frequency
$C_0$	mass $\times$ peak acceleration
m	mass
$\Omega$	factor equal to $(1 + \nu/2\pi)$
D	amplitude of transverse pulse
$c_g$	group velocity

APPENDIX A

SOLUTION OF THE DYNAMIC EQUATION FOR THE ELASTIC-  
VISCOELASTIC MODEL WHEN EXCITED BY A HALF-CYCLE  
SINE PULSE

The equation of motion for the Elastic-Viscoelastic Model is:

$$\eta \frac{\partial \epsilon}{\partial t} + (2E)\epsilon = \sigma \quad (1)$$

rearranging

$$\frac{\partial \epsilon}{\partial t} + \frac{(2E)}{\eta} \epsilon = \frac{\sigma}{\eta}$$

or

$$\frac{\partial \epsilon}{\partial t} + \frac{E'}{\eta} \epsilon = \frac{\sigma}{\eta}$$

taking the Laplace transform of this equation

$$sF(s) + \frac{E'}{\eta} F(s) - f(0) = \frac{1}{\eta} F_{\sigma}(s) \quad (2)$$

the stress generated by the half cycle sine pulse is  $m a(t) = m a_p \sin \frac{\pi}{\tau} t$  or

$$F(t) = C_0 \sin\left(\frac{\pi}{\tau} t\right)$$

where

(3)

$$C_0 = m a_p$$

taking the Laplace transform of the force equation yields

$$F_{\sigma}(s) = C_0 \frac{\pi}{\tau} \left( \frac{1}{s^2 + \left(\frac{\pi}{\tau}\right)^2} \right) \quad (4)$$

substituting equation (4) into equation (2) yields:

$$sF(s) + \frac{E'}{\eta} F(s) - f(0) = \frac{1}{\eta} C_0 \frac{\pi}{\tau} \left( \frac{1}{s^2 + \left(\frac{\pi}{\tau}\right)^2} \right)$$

rearranging and solving for F(s) gives

$$F(s) = \frac{f(0) + \frac{C_0 \pi}{\eta \tau} \frac{1}{s^2 + (\frac{\pi}{\tau})^2}}{s + \frac{E'}{\eta}}$$

$$F(s) = \frac{f(0)}{s + \frac{E'}{\eta}} + \frac{C_0}{\eta} \left( \frac{\pi}{\tau} \right) \left[ \frac{1}{(s + \frac{E'}{\eta}) (s^2 + \frac{\pi}{\tau})^2} \right] \quad (5)$$

The time dependent strain is found by taking the inverse transform of the above equation:

$$\epsilon(t) = \mathcal{L}F^{-1}(s) = \epsilon_0 \mathcal{L}^{-1} \left[ \frac{1}{s + \frac{E'}{\eta}} \right] + \frac{C_0}{\eta} \left( \frac{\pi}{\tau} \right) \mathcal{L}^{-1} \left[ \frac{1}{(s + \frac{E'}{\eta}) (s^2 + \frac{\pi}{\tau})^2} \right]$$

If we neglect the residual strain on the system prior to the application of the load ( $\epsilon_0 = 0$ ) the above expression simplifies to

$$\epsilon(t) = \frac{C_0}{\eta} \frac{\pi}{\tau} \mathcal{L}^{-1} \left[ \frac{1}{(s + \frac{E'}{\eta}) (s^2 + (\frac{\pi}{\tau})^2)} \right]$$

expanding the fraction in bracket by partial fractions yields:

$$\epsilon(t) = \frac{C_0}{\eta} \left( \frac{\pi}{\tau} \right) \mathcal{L}^{-1} \left[ \frac{K_1}{s + \frac{E'}{\eta}} + \frac{K_2}{s + i(\frac{\pi}{\tau})} + \frac{K_3}{s - i(\frac{\pi}{\tau})} \right]$$

performing the inverse transform yields:

$$\epsilon(t) = \frac{C_0}{\eta} \left( \frac{\pi}{\tau} \right) \left[ K_1 e^{-\left(\frac{E'}{\eta}\right)t} + K_2 e^{-i\left(\frac{\pi}{\tau}\right)t} + K_3 e^{i\left(\frac{\pi}{\tau}\right)t} \right] \quad (6)$$

where

$$i = \sqrt{-1}$$

$$K_1 = \frac{1}{\left(\frac{E'}{\eta}\right)^2 + \left(\frac{\pi}{\tau}\right)^2}$$

$$K_2 = \frac{1}{2\frac{\pi}{\tau} \left(-\frac{\pi}{\tau} + \frac{E'}{\eta}\right)}$$

$$K_3 = \frac{1}{2\frac{\pi}{\tau} \left(-\frac{\pi}{\tau} + i\frac{E'}{\eta}\right)}$$

substituting these constants into equation (6) yields

$$\epsilon(t) = \frac{C_0}{\eta} \left(\frac{\pi}{\tau}\right) \left[ \frac{e^{-\left(\frac{E'}{\eta}\right)t}}{\left(\frac{\pi}{\tau}\right)^2 + \left(\frac{E'}{\eta}\right)^2} + \frac{e^{-i\left(\frac{\pi}{\tau}\right)t}}{2\frac{\pi}{\tau} \left(-\frac{\pi}{\tau} - i\frac{E'}{\eta}\right)} + \frac{e^{i\left(\frac{\pi}{\tau}\right)t}}{2\frac{\pi}{\tau} \left(-\frac{\pi}{\tau} + i\frac{E'}{\eta}\right)} \right]$$

rearrangement along with using the relations;  $\cos \frac{\pi}{\tau} t = 1/2 \left( e^{i\left(\frac{\pi}{\tau}\right)t} + e^{-i\left(\frac{\pi}{\tau}\right)t} \right)$  and

$\sin\left(\frac{\pi}{\tau}\right)t = -i(1/2) \left( e^{i\left(\frac{\pi}{\tau}\right)t} - e^{-i\left(\frac{\pi}{\tau}\right)t} \right)$  yield the final expression for the strain:

$$\epsilon(t) = \frac{C_0}{\eta} \left[ \frac{\frac{E'}{\eta} \sin\left(\frac{\pi}{\tau}\right)t - \frac{\pi}{\tau} \cos\left(\frac{\pi}{\tau}\right)t + \frac{\pi}{\tau} e^{-\left(\frac{E'}{\eta}\right)t}}{\left(\frac{\pi}{\tau}\right)^2 + \left(\frac{E'}{\eta}\right)^2} \right] \quad (7)$$

The "dynamic" modulus is

$$\phi = \frac{\sigma(t)}{\epsilon(t)} = \frac{C_0 \sin\left(\frac{\pi}{\tau}\right)t}{\frac{C_0}{\eta} \left[ \frac{\frac{E'}{\eta} \sin\left(\frac{\pi}{\tau}\right)t - \frac{\pi}{\tau} \cos\left(\frac{\pi}{\tau}\right)t + \frac{\pi}{\tau} e^{-\left(\frac{E'}{\eta}\right)t}}{\left(\frac{\pi}{\tau}\right)^2 + \left(\frac{E'}{\eta}\right)^2} \right]}$$

rearrangement yields

$$\phi = \left[ \frac{\left(\frac{\pi}{\tau}\right)^2 + \left(\frac{E'}{\eta}\right)^2 \eta \sin\left(\frac{\pi}{\tau}\right)t}{\frac{E'}{\eta} \sin\left(\frac{\pi}{\tau}\right)t - \frac{\pi}{\tau} \cos\left(\frac{\pi}{\tau}\right)t + \frac{\pi}{\tau} e^{-\left(\frac{E'}{\eta}\right)t}} \right]$$

In this case, the burst strength was to be measured and the maximum value of the "dynamic modulus" was of interest. This occurs when  $\sin\left(\frac{\pi}{\tau}\right)t = 1$  or  $t = \frac{\tau}{2}$ , substituting in this value into  $\phi$  gives

$$\phi = \left[ \frac{\left(\frac{\pi}{\tau}\right)^2 + \left(\frac{E'}{\eta}\right)^2}{\frac{E'}{\eta} + \frac{\pi}{\tau} e^{-\left(\frac{E'}{\eta}\right)\frac{\tau}{2}}} \right] \eta \quad (8)$$

when

$$\frac{\pi}{\tau} \gg \frac{E'}{\eta} \text{ and } e^{-\left(\frac{E'}{\eta}\right)\frac{\tau}{2}} \cong 1$$

equation (8) can be simplified to

$$\phi = \left(\frac{\pi}{\tau}\right) \eta$$

## APPENDIX B

### PROPAGATION OF STRESS WAVE IN A FLAT PLATE

Figure B shows the forces acting on a small element of the plate of radial dimension  $\Delta x$ . In this system the bending moment  $M$  is balanced by shearing forces  $f$  acting perpendicular to the plate thickness.

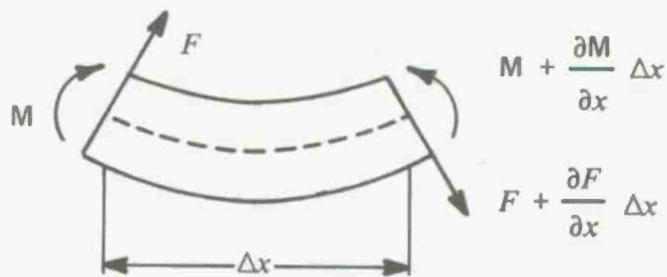


Figure B

From Newton's second law, the equation of motion for the plate is:

$$\Delta x \rho A \frac{\partial^2 w}{\partial t^2} = f + \frac{\partial f}{\partial x} \Delta x - f$$

or

(1)

$$\rho A \frac{\partial^2 w}{\partial t^2} = \frac{\partial f}{\partial x}$$

the relationship between shearing force and bending moment is

$$f = \frac{\partial M}{\partial x}$$

where

$$M = \phi I \left( \frac{\partial^2 w}{\partial x^2} + \frac{\partial^2 w}{\partial y^2} \right)$$

or

$$f = \phi I \frac{\partial}{\partial X} \left( \frac{\partial^2 w}{\partial x^2} + \frac{\partial^2 w}{\partial y^2} \right) \equiv \phi I \frac{\partial}{\partial x} \left( \frac{\partial \epsilon_x}{\partial x} - \frac{\partial \epsilon_y}{\partial y} \right) \quad (2)$$

where  $w$  is the displacement,  $x$  is the radial component,  $y$  is the circumferential component and the strain is defined as equal to

$$\epsilon_x = \frac{\partial w}{\partial x}, \quad \epsilon_y = \frac{\partial w}{\partial y}$$

The relationship between the radial and circumferential components are:

$$\frac{\epsilon_y}{\epsilon_x} = \nu$$

and for the circular flat plate

$$y = 2\pi x$$

therefore

$$\frac{\partial \epsilon_y}{\partial y} = \nu \frac{\partial \epsilon_x}{\partial y} = \nu \frac{\partial \epsilon_x}{\partial x} \frac{\partial x}{\partial y} = \frac{\nu}{2\pi} \frac{\partial \epsilon_x}{\partial x}$$

substituting the preceding equation into equation (2) yields

$$f = \phi I \frac{\partial}{\partial x} \left( \frac{\partial \epsilon_x}{\partial x} + \frac{\nu}{2\pi} \frac{\partial \epsilon_x}{\partial x} \right) = \phi I \left( 1 + \frac{\nu}{2\pi} \right) \frac{\partial^2 \epsilon_x}{\partial x^2}$$

or

$$f = \phi I \left( 1 + \frac{\nu}{2\pi} \right) \frac{\partial^3 w}{\partial x^3} \quad (3)$$

substituting into the equation of motion (1) yields

$$\frac{\partial^2 w}{\partial t^2} = \left(\frac{\phi}{\rho}\right)\left(\frac{1}{A}\right)\left(1 + \frac{\nu}{2\pi}\right)\frac{\partial^4 w}{\partial x^4}$$

let

$$c_0^2 = \left(\frac{\phi}{\rho}\right), \quad K^2 = \left(\frac{1}{A}\right), \quad \Omega^2 = \left(1 + \frac{\nu}{2\pi}\right)$$

substituting these parameters into the equation of motion yield

$$\frac{\partial^2 w}{\partial t^2} = c_0^2 K^2 \Omega^2 \frac{\partial^4 w}{\partial x^4}$$

The solution to the above equation is  $w = D\cos(pt - \alpha x)$  or  $w = D\sin(pt - \alpha x)$  which are the equations for a transverse pulse where  $\alpha = \frac{2\pi}{\Lambda}$ ,  $p = \frac{2\pi c}{\Lambda}$  and  $\Lambda$  is the wave length of the pulse and  $c$  is the phase velocity of the stress wave.

Substituting either one of the above equations for  $w$  into the equation of motion gives,

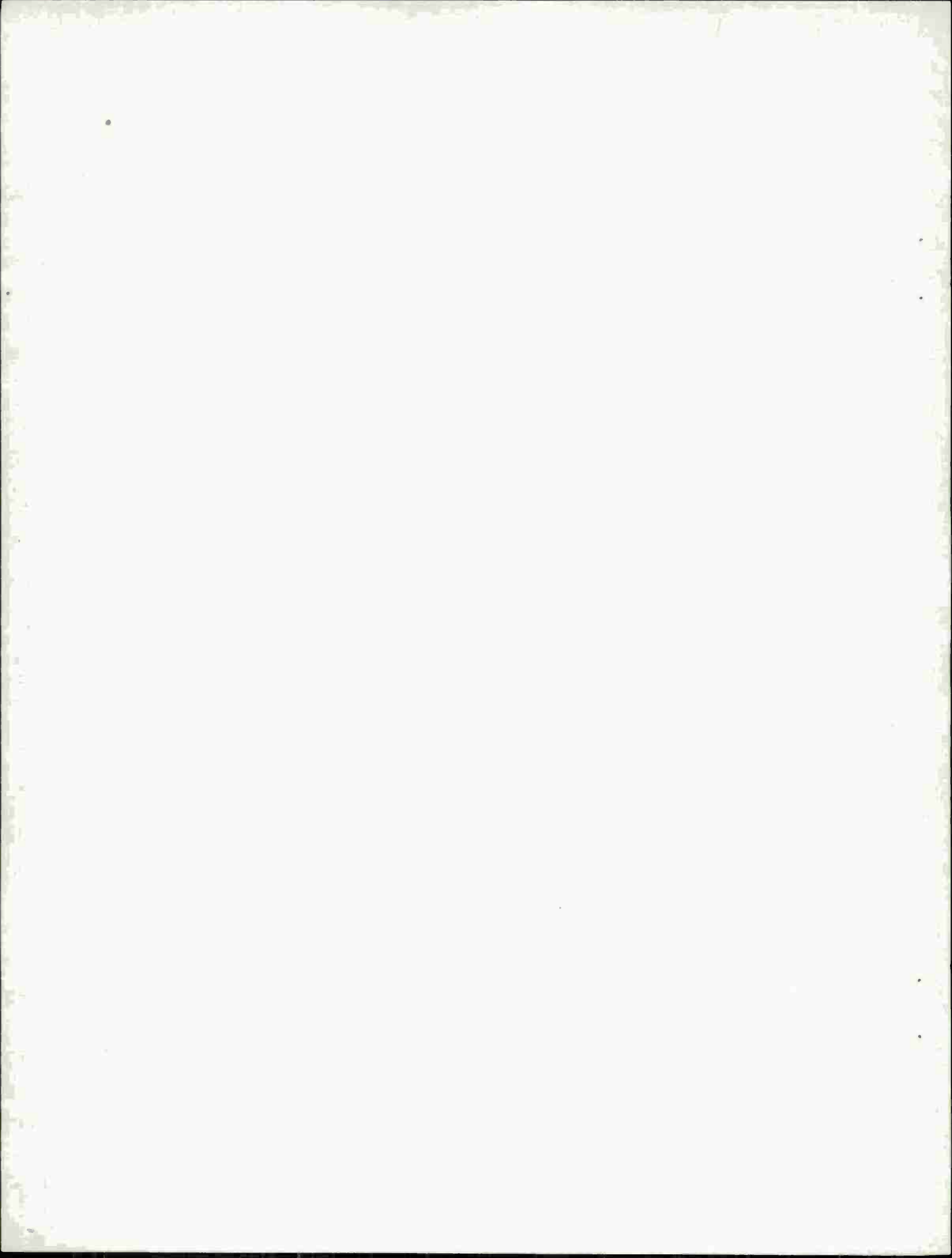
$$p^2 = c_0^2 K^2 \alpha^4 \Omega^2$$

$$c = c_0 \left(\frac{2\pi K \Omega}{\Lambda}\right)$$

From the equation of continuity, that is, the displacement of the disk must equal the total elongation of the disk or  $v t = \epsilon x$ . Rearranging this equation give  $v = \frac{x}{t} \epsilon$  where Von Karman showed that  $\frac{x}{t}$  is equal to the velocity of the wave propagation in the plastic region. In this case the velocity of wave propagation ( $C_g$ ) refers to the velocity with which a packet of waves is propagated, the wavelengths of which are close to  $\Lambda$ . This is related to the phase velocity ( $c$ ) by  $C_g = 2c$ .

Finally at the point of rupture

$$\sigma = \phi \epsilon = \phi \frac{v}{c_g} = c_0 \nu \rho \left(\frac{\Lambda}{4\pi K \Omega}\right)$$



APPENDIX C

CALCULATION OF THE AISI 1018 LOW-CARBON STEEL

CIRCULAR FLAT PLATE

From the stress-strain diagram (figure 6)

$$\Delta\sigma = 65,000 - 41,700 = 23,300 \text{ psi}$$

$$\epsilon_{o,\nu} = (\epsilon_{o,\text{total}} - \epsilon_{o,E})$$

$$\epsilon_{o,\text{total}} = 0.30$$

$$\epsilon_{o,E} = 0.02$$

$$\epsilon_{o,\nu} = 0.30 - 0.02 = 0.28$$

$$\frac{\partial \epsilon_o}{\partial t} = \text{cross head rate} \times \text{distance between jaws}$$

$$= \frac{0.1 \text{ in/in/min}}{1 \text{ in}} \times 2 \text{ in} \times \frac{1 \text{ min}}{60 \text{ sec}} = 0.00333 \text{ sec}^{-1}$$

From Calibration Chart (figure 5, pad 31-200-085-350) half sine wave period,  $\tau = 0.007 \text{ sec}$ .

From test data

$$\text{Acceleration at shear} = 145 \text{ g}$$

$$\text{Disk radius} = 1 \text{ in}$$

$$\text{Disk thickness} = 0.0153 \text{ in}$$

Handbook Data

$$E = 30,000,000 \text{ psi}$$

$$\rho = 0.284 \text{ lb/in}^3$$

$$\nu = 0.29$$

(1) Calculation of dynamic modulus:

The viscous parameter  $\eta$ , was calculated by substituting the values given in figure 6 into the equation given in figure 2 of the body of this report, that is:

$$\eta = \frac{23,300}{.00333} (1 + 0.28) = 8,956,200 \frac{\text{lb-sec}}{\text{in}^2}$$

$$\frac{E}{\eta} = \frac{30,000,000}{8,956,200} = 3.35 \text{ sec}^{-1}$$

$$\frac{\pi}{\tau} = \frac{3.1416}{0.007} = 448.8 \text{ sec}^{-1}$$

$$\frac{E}{\eta} \frac{\tau}{2} = 3.35 \times \frac{0.007}{2} = 0.0117$$

since  $\frac{\pi}{\tau} \gg \frac{E}{\eta}$  and  $e^{-0.0117} \cong 1$ , the simplified form was used,

$$\phi_E = \left(\frac{\pi}{\tau}\right) \eta = 448.8 \times 8,956,200 = 4,018,500,000 \text{ psi}$$

However, the plate was in shear while the data were from tensile tests. This was accounted for by using the following relation:

$$\phi_s = \frac{\phi_E}{2(1+\nu)} = \frac{4,019,500,000}{2(1+0.29)} = 1,558,000,000 \text{ psi}$$

or

$$224,352,000,000 \text{ psf (lb/ft}^2\text{)}$$

(2) Calculation of stress wave parameters where:

- the impact velocity\*  $v = a_p \frac{\tau}{\pi}$ , in this case  $a_p = 145 \text{ gs}$  acceleration

or

\*See Appendix D for response characteristics of the pulse

$$v = 145 \text{ g} \times 32.17 \text{ ft/sec}^2 \times \frac{(0.007 \text{ sec})}{3.1416}$$

$$= 10.39 \text{ ft/sec}$$

- the half wave length  $\Lambda = v\tau$

$$\Lambda = 10.39 \text{ ft/sec} \times 0.007 \text{ sec} = .0727 \text{ ft}$$

$$\text{- the radius of gyration } K = \left(\frac{I}{A}\right)^{1/2} = \left(\frac{\rho\pi b \frac{r^4}{4}}{2\pi br}\right)^{1/2} = \left(\frac{\rho r^3}{8}\right)^{1/2}$$

The radius of gyration is

$$K = \left(\frac{0.284 \times 1^3}{8}\right)^{1/2} = 0.188$$

$$-\Omega = \left(1 + \frac{v}{2\pi}\right)^{1/2} = \left(1 + \frac{0.29}{2\pi}\right)^{1/2} = 1.023$$

$$\begin{aligned} \text{- the propagation velocity } c_o &= \left(\frac{\phi_s}{\rho}\right)^{1/2} \\ &= \left(\frac{224,352,000,000}{0.284 \times 12^3}\right)^{1/2} \\ &= 21,381 \text{ ft/sec} \end{aligned}$$

(3) Calculation of plate stress and pressure – from Appendix B:

$$\begin{aligned} \sigma &= c_o \rho v \left(\frac{\Lambda}{4\pi K \Omega}\right) \\ &= 21,381 \times 490.75 \times 10.39 \frac{0.0727}{4 \times 3.1416 \times 0.188 \times 1.023} \\ &= 3,279,396 \text{ psf or } 22,774 \text{ psi stress} \end{aligned}$$

The pressure P is equal to the total load (stress  $\times$  circumference) divided by the total area of the

plate, 
$$P = \frac{\sigma \times 2\pi r b}{\pi r^2} = \sigma \left( \frac{2b}{r} \right)$$

for a 0.0153-inch-thick plate having a 1-inch radius:

$$P = 22,774 \left( \frac{2 \times 0.0153}{1} \right) = 697 \text{ psi pressure.}$$

## APPENDIX D

### THE RESPONSE CHARACTERISTICS OF THE HALF-CYCLE SINE PULSE

#### ACCELERATION

$$a(t) = a_p \sin\left(\frac{\pi}{\tau}\right)t$$

taking the Laplace transform

$$s F(v) - f(0) = a_p \frac{\pi}{\tau} \left[ \frac{1}{\left(s^2 + \frac{\pi}{\tau}\right)^2} \right]$$

$$F(v) = \frac{f(0)}{s} + a_p \frac{\pi}{\tau} \left[ \frac{1}{\left(s\left(s^2 + \frac{\pi}{\tau}\right)^2\right)} \right]$$

taking the inverse transform

$$v(t) = v_0 t + a_p \frac{\pi}{\tau} \frac{1}{\left(\frac{\pi}{\tau}\right)^2} \left(1 - \cos\left(\frac{\pi}{\tau}\right)t\right)$$

$$= v_0 t + a_p \left(\frac{\tau}{\pi}\right) \left(1 - \cos \frac{\pi}{\tau} t\right)$$

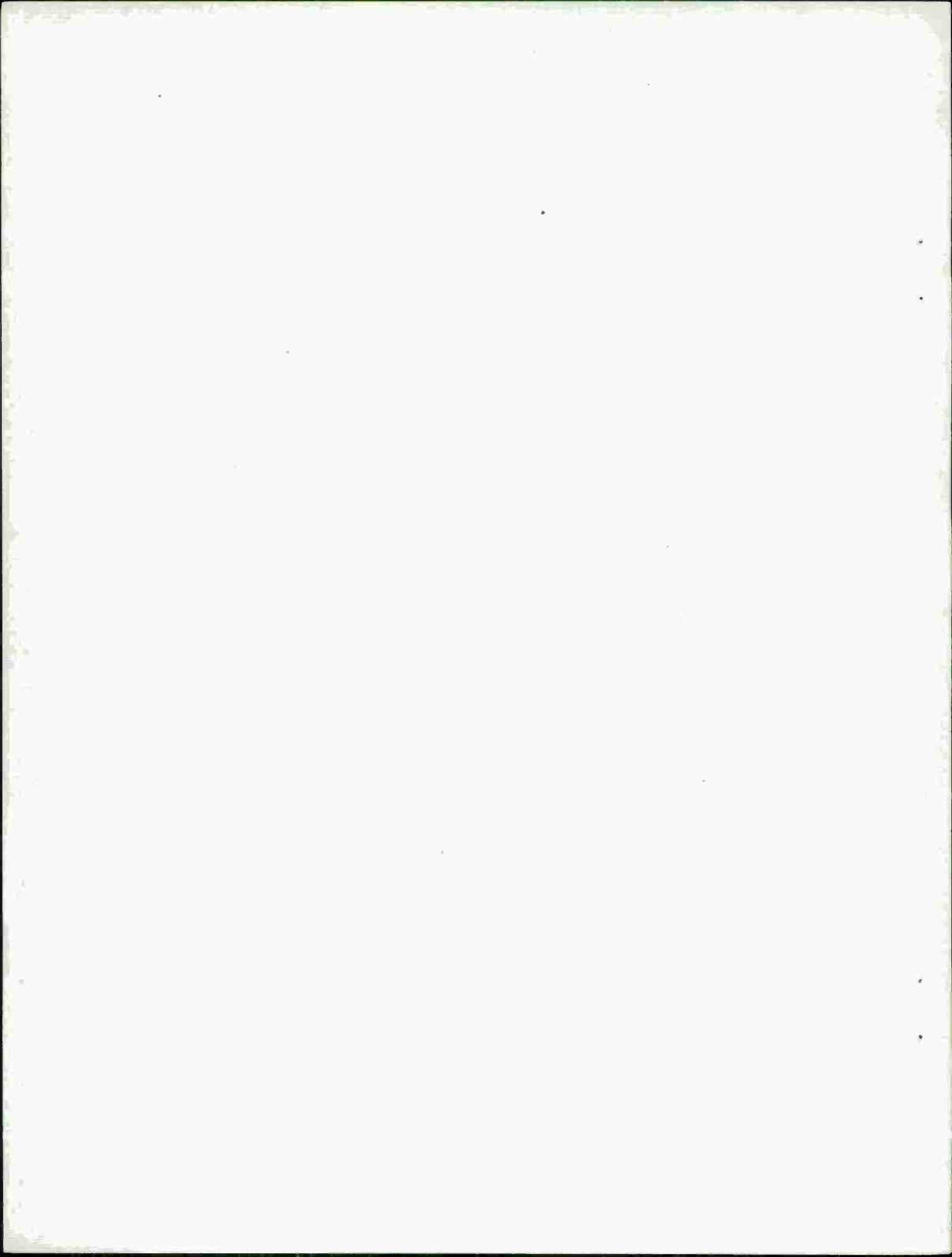
let

$$v_0 = 0$$

$$v(t) = a_p \left(\frac{\tau}{\pi}\right) \left(1 - \cos \frac{\pi}{\tau} t\right)$$

the velocity is maximum at  $t = \frac{\tau}{2}$

having  $v_m = a_p \left(\frac{\tau}{\pi}\right)$ .



DISTRIBUTION LIST 2

Names	Copies	Names	Copies
CHEMICAL SYSTEMS LABORATORY		US Army Research and Standardization	
SAFETY OFFICE		Group (Europe)	1
Attn: DRDAR-CLF	1	Attn: Chief, Chemistry Branch	
PLANNING & TECHNOLOGY OFFICE		Box 65, FPO New York 09510	
Attn: DRDAR-CLR-L	4	Commander	
AUTHOR'S COPIES: Munitions Division	10	HQ US Army Medical Command, Europe	
		Attn: AEMPM	1
		APO New York 09403	
BIOMEDICAL LABORATORY		US ARMY MATERIEL DEVELOPMENT AND	
Attn: DRDAR-CLL-B	1	READINESS COMMAND	
Attn: DRDAR-CLL-MC	1	Commander	
CB DETECTION & ALARMS DIVISION		US Army Materiel Development and Readiness Command	
Attn: DRDAR-CLC-C	1	Attn: DRCLDC	1
DEVELOPMENTAL SUPPORT DIVISION		Attn: DRCSF-P	1
Attn: DRDAR-CLJ-R	3	5001 Eisenhower Ave	
Attn: DRDAR-CLJ-L	3	Alexandria, VA 22333	
ENVIRONMENTAL TECHNOLOGY DIVISION		Office of the Project Manager for Chemical Demilitarization	
Attn: DRDAR-CLT-E	1	and Installation Restoration	
MUNITIONS DIVISION		Attn: DRCPM-DR-T	2
Attn: DRDAR-CLN	1	Aberdeen Proving Ground, MD 21010	
PHYSICAL PROTECTION DIVISION		Project Manager Smoke/Obscurance	
Attn: DRDAR-CLW-P	1	Attn: DRCPM-SMK-M	1
RESEARCH DIVISION		Aberdeen Proving Ground, MD 21005	
Attn: DRDAR-CLB	1	Human Engineering Laboratory HFE Detachment	
Attn: DRDAR-CLB-B	1	Attn: DRXHE-EA	1
Attn: DRDAR-CLB-C	1	Building E3220	
Attn: DRDAR-CLB-P	1	APG-Edgewood Area	
Attn: DRDAR-CLB-R	1	Commander	
Attn: DRDAR-CLB-T	1	US Army Missile Research and Development Command	
Attn: DRDAR-CLB-TE	1	Redstone Scientific Information Center	
SYSTEMS ASSESSMENTS OFFICE		Attn: DRDMI-TBD	1
Attn: DRDAR-CLY	1	Redstone Arsenal, AL 35809	
Attn: DRDAR-CLY-R	1	Director	
DEPARTMENT OF DEFENSE		DARCOM Field Safety Activity	
Administrator		Attn: DRXOS-C	1
Defense Documentation Center		Charlestown, IN 47111	
Attn: Accessions Division (DDC-TC)	12	US ARMY ARMAMENT RESEARCH AND	
Cameron Station		DEVELOPMENT COMMAND	
Alexandria, VA 22314		Commander	
Director		US Army Armament Research and Development Command	
Defense Intelligence Agency		Attn: DRDAR-LCA	1
Attn: DB-4G1	1	Attn: DRDAR-LCE	2
Washington, DC 20301		Attn: DRDAR-LCE-M	1
DEPARTMENT OF THE ARMY		Attn: DRDAR-LCF	1
HQDA (DAMO-SSC)		Attn: DRDAR-LCU	1
WASH DC 20310	1	Attn: DRDAR-SCA-PP	1
Deputy Chief of Staff for Research,		Attn: DRDAR-SCN	1
Development & Acquisition		Attn: DRDAR-SCP-A	1
Attn: DAMA-CSM-CM	1	Attn: DRDAR-SER	1
Attn: DAMA-ARZ-D	1	Attn: DRDAR-TSS	2
Washington, DC 20310		Dover, NJ 07801	

DISTRIBUTION LIST 2 (Contd)

Names	Copies	Names	Copies
Director Ballistic Research Laboratory Attn: DRDAR-TSB-S Building 328 Aberdeen Proving Ground, MD 21005	1	Commanding Officer Naval Weapons Support Center Attn: Code 5042/Dr. B. E. Doua Crane, IN 47522	1
CDR, APG USA ARRADCOM Attn: DRDAR-GCL Aberdeen Proving Ground, MD 21010	1	DEPARTMENT OF THE AIR FORCE HQ Foreign Technology Division (AFSC) Attn: PDRR Wright-Patterson AFB, OH 45433	1
US ARMY ARMAMENT MATERIEL READINESS COMMAND Commander US Army Armament Materiel Readiness Command Attn: DRSAR-ASN Attn: DRSAR-IMB-C Rock Island, IL 61201	1 1	Commander Aeronautical Systems Division Attn: ASD/AELD Wright-Patterson AFB, OH 45433	1
Commander US Army Dugway Proving Ground Attn: Technical Library, Docu Sect Dugway, UT 84022	1	HQ AFISC/SEV Norton AFB, CA 92409	1
Commander Rocky Mountain Arsenal Attn: SARRM-QA Commerce City, CO 80022	1	OUTSIDE AGENCIES Battelle, Columbus Laboratories Attn: TACTEC 505 King Avenue Columbus, OH 43201	1
Commander Pine Bluff Arsenal Attn: SARPB-ETA Pine Bluff, AR 71611	1	Director of Toxicology National Research Council 2101 Constitution Ave, NW Washington, DC 20418	1
US ARMY TRAINING & DOCTRINE COMMAND Commandant US Army Infantry School Attn: NBC Division Fort Benning, GA 31905	1	ADDITIONAL ADDRESSEES US Public Health Service Room 17A-46 (CPT Osheroff) 5600 Fishers Lane Rockville, MD 20857	1
Commandant US Army Military Police School/Training Center Attn: ATZN-TDP-C Fort McClellan, AL 36205	1	Commander US Army Environmental Hygiene Agency Attn: Librarian, Bldg 2100 Aberdeen Proving Ground, MD 21010	1
Commander US Army Infantry Center Attn: ATSH-CD-MS-C Fort Benning, GA 31905	1	Commander DARCOM, STITEUR Attn: DRXST-ST1 Box 48, APO New York 09710	1
US ARMY TEST & EVALUATION COMMAND Commander US Army Cold Regions Test Center Attn: STECR-TD APO Seattle, WA 98733	1	Commander US Army Science & Technology Center-Far East Office APO San Francisco 96328	1
DEPARTMENT OF THE NAVY Chief of Naval Research Attn: Code 443 800 N. Quincy Street Arlington, VA 22217	1	HQDA DASG-RDZ (SGRD-PL) WASH DC 20314	1
		AMREL/MEB Wright-Patterson AFB, OH 45433	1
		Commander USEUCOM Attn: ECJ%-O/LTC James H. Alley APO, NY 09128	1

